Nanoscale

Accepted Manuscript

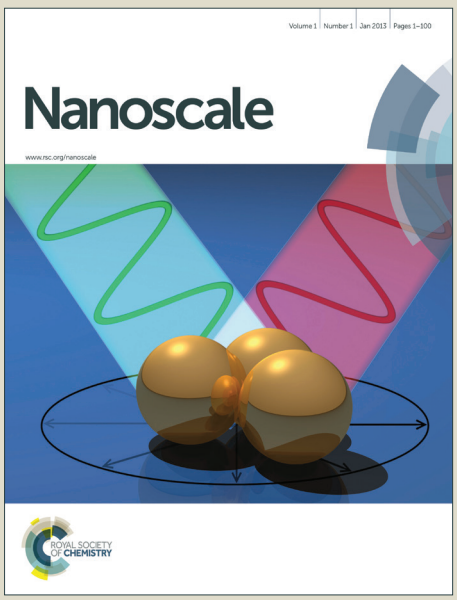

This is an *Accepted Manuscript*, which has been through the Royal Society of Chemistry peer review process and has been accepted for publication.

Accepted Manuscripts are published online shortly after acceptance, before technical editing, formatting and proof reading. Using this free service, authors can make their results available to the community, in citable form, before we publish the edited article. We will replace this *Accepted Manuscript* with the edited and formatted *Advance Article* as soon as it is available.

You can find more information about *Accepted Manuscripts* in the Information for Authors.

Please note that technical editing may introduce minor changes to the text and/or graphics, which may alter content. The journal's standard Terms & Conditions and the Ethical guidelines still apply. In no event shall the Royal Society of Chemistry be held responsible for any errors or omissions in this *Accepted Manuscript* or any consequences arising from the use of any information it contains.

ROYAL SOCIETY OF CHEMISTRY

www.rsc.org/nanoscale

Please do not adjust margins

Journal Name

ARTICLE

Micro-dressing of Carbon Nanotubes Array with MoS_2 Gauze

Sharon Xiaodai Lim[a], Kah Whye Woo[b], Junju Ng[b], Junpeng Lu[a], Siu Yi Kwang[a], Zheng Zhang[c], Eng Soon Tok[a], Chorng-Haur Sow[a*]

Received 00th January 20xx,
Accepted 00th January 20xx

DOI: 10.1039/x0xx00000x

www.rsc.org/

Few-layer MoS_2 film has been successfully assembled over array of CNTs. Using different focused laser beam with different wavelengths, site selective patterning of either the MoS_2 film or the supporting CNTs array is achieved. This paves the way for applications and investigations into the fundamental properties of the hybrid MoS_2/CNTs material with controlled architecture. Through Raman mapping, straining and electron doping of MoS_2 film as a result of interaction with the supporting CNTs array are detected. Role of the MoS_2 film was further emphasized with lower work function being detected from Ultra-violet Photoelectron Spectrsocopy (UPS) measurements of the hybrid material, compared to the CNTs array. Effect of the changes in the work function was illustrated through optoelectronic behavior of the hybrid material. At 0V, 3.49nA of current is measured upon illuminating the sample with a broad laser beam emitting laser light with a wavelength of 532nm. With strong response to external irradiation of different wavelength, and changes to the power of the excitation source, the hybrid material has shown potential for applications in optoelectronics devices.

Introduction

The wonder of hybrid material lies in its ability to possess the advantages of its individual components, and at the same time present new properties and functions for practical applications. From zero-dimensional (0D) nanoparticles[1] to 3D nanofoams/networks,[2] from metals[3] to polymer,[4] there is a tremendous range of variety to which these hybrid materials could be created. Of these materials, we selected two of the most extensive studied nanomaterials, namely, molybdenum disulfide (MoS_2) and multi-walled carbon nanotubes (CNTs) to create functional hybrid materials. MoS_2 film is a typical two-dimensional (2D) system that exhibits thickness-dependent tunable bandgap and multi-walled CNTs are one-dimensional (1D) and metallic. Creating controlled three-dimensional (3D) micro-structures out of these two materials with vast differences in their intrinsic properties would be very interesting and the success of which would provide a good handle to tailor-made micro-architecture with unique performance.

MoS_2 in its monolayer form had gained vast popularity in the field of research with potential applications due to its direct bandgap property.[5, 6] It is only very recently that few-layer MoS_2 with its promising semiconducting characteristics and potential applications in nano-electronics and optoelectronics had allowed it to outshine its monolayer counterpart.[7, 8] At room temperature, metallic multi-walled CNTs are known to allow ballastic transport of charge carrier over a distance of > 1μm. Not only so, these nanotubes have been found to be able to withstand a current density as high as 10^{11}-10^{12} A cm^{-2}.[9, 10] This is 6 order of magnitude higher than those reported from other nanowires such as Bi_2S_3 nanowires, whose current density was reported to be 10^5 A cm^{-2}.[11] As such, we believe that these CNTs are one of the most promising material that offers highly efficient transportation of charge carriers at room temperature. In a recent work by Zhang *et al.,* they highlighted dominating photovoltaic effect at few-layer MoS_2-metal interface.[8] This suggests that in tailoring 3D micro-structures out of the MoS_2 films and CNTs, multiple contacts between the few-layer MoS_2 film and metallic MWNTs could essentially encourage charge transfer of photo-induced electron-hole pairs generated at the interface of these two materials, to the metallic CNTs in an effective manner.

It would even be better if there exists a flexibility to craft either the MoS_2 film or the underlying CNTs array into any desired shape and size. Patterning 2D/3D materials into specific spatial arrangements and geometries had long been a pre-requisite for the study of both fundamental properties of the materials, as well as for practical applications in electronic devices. As such, the availability of such tailoring capability will be most useful in leveraging the optoelectronic property of this hybrid material for photovoltaic and other optoelectronic applications. With the two materials having distinct responses to laser beam with different wavelength (CNTs response well to 660nm laser[12] while MoS_2 was found to interact well with

[a] *Department of Physics, Blk S12, Faculty of Science, National University of Singapore, 2 Science Drive 3, Singapore 117542.*
[b] *Dunman High School, 10 Tanjong Rhu Road, Singapore 436895.*
[c] *Institute of Materials Research and Engineering, A*STAR (Agency for Science, Technology and Research), 3 Research Link, 117602, Singapore*

† Address correspondence to Prof. C. H. Sow. Phone: (+65) 65162957. Fax: (+65) 67776126. E-mail: physowch@nus.edu.sg.
See DOI: 10.1039/x0xx00000x

Nanoscale Accepted Manuscript

Please do not adjust margins

532nm laser[13]), this offers us the feasibility to carry out post-synthesized and post-assembly laser initiated patterning of the hybrid sample to further create micro-devices for better functionality.

Furthermore, controlled straining has been well established as a viable tool in bandgap engineering of 2D TMD films. Given the ease of using fluid to induce controlled formations of micro- and nano-structures out of these extremely flexible CNTs,[14, 15] the 3D hybrid material thus offers a good opportunity for detailed and systematic study of the effect of real-time changes to structural induced straining of MoS_2 by fluid initiated controlled assembly of laser patterned CNT structures.

To date, one common method for the creation of MoS_2 and CNTs hybrid structure is through hydrothermal process,[16, 17] through which, MoS_2 over layers anchored on coaxial CNTs were created. However, the layers were not evenly coated to form the core-shell CNT/MoS_2 structures. Furthermore, given that the CNTs used are randomly dispersed, additional work is required to create a device from these materials. Moreover, given the coaxial nature of the hybrid formed, it will not be possible to tailor the shape and size of the MoS_2 film for device fabrications.

Herein, we present a simple yet efficient method to cover vertically aligned multi-walled CNTs under a veil of few-layer n-type MoS_2 film. Not only does the 3D hybrid material created using this method display excellent optoelectronic property at low applied voltage, spreading of the MoS_2 film over the supporting CNT scaffolds also allow the possibility of using a low power focused laser beam to pattern the film into any desired shape and size, without any destruction to the underlying CNTs. The hybrid material thus presents a route towards the creation of site specific metallic (CNTs) and semi-conducting (MoS_2/CNTs) hybrid structures. This unique way of assembling and tailoring MoS_2 film on CNTs thus eased the way for the development of site selective optoelectric conversion in 3D microelectronic devices that can readily be handled for measurements and characterizations.

Experimental

Growth of CNTs

Aligned multi-walled CNTs are grown on 5mm x 5mm clean n-type silicon ((100) Si) substrates. Before growth, a layer of iron film is coated on the substrates using a magnetron sputtering system (Model: RF Magnetron Denton Discovery 18). The coating serves as catalyst and the sputtering rate is 4nm/min lasting for 3.25mins. The CNTs are synthesized using a Plasma Enhanced Chemical Vapor Deposition (PECVD) and details of the growth process are reported elsewhere.[18]

Growth of Few-layer n-type MoS2 Film

0.5-5mg of $MoCl_5$ powder is loaded in a ceramic boat and placed at the center of a horizontal tube furnace. 1g of sulfur powder is placed at the upstream of the furnace and the substrate (Si/SiO_2) is placed beside the $MoCl_5$ source. To initiate the growth process, temperature of the furnace is increased to 900^{o}C at the rate of 40^{o}C/min. The sulfur powder is heated separately to 200^{o}C, and the vapor is carried by He gas to the center at a constant flow rate of 20sccm with the pressure maintained at 1Torr. The furnace is maintained at 900^{o}C for 15min before cooling to room temperature. Adjusting the amount of precursor control the thickness of the MoS_2 films. To improve the crystalline quality, the samples are annealed in sulfur ambient.[19]

Floating of Few-layer MoS2 Film from Substrate

Firstly, a protection layer of PMMA resist (~350nm) is spin-coated onto the MoS_2 film and heated at 180^{o}C. Scratches are introduced onto the corner of the substrate before placing the sample in a solution of diluted potassium hydroxide in de-ionised (DI) water (ratio of 1:5) and rinsed in DI water. During the etching process, the solution is heated at 125^{o}C. The MoS_2 film is transferred on to glass and then floated on top of water in a beaker.

Ultra-violet Photoelectron Spectroscopy (UPS)

Samples are analyzed by VG ESCALAB 220i-XL X-ray photoelectron spectroscopy (XPS) system equipped with an ultra-violet gas discharge lamp as excitation sources. The electron analyser is calibrated with polycrystalline gold, silver and copper standard samples by setting the Au $4f_{7/2}$, Ag $3d_{5/2}$ and Cu $2p_{3/2}$peaks at binding energies of 83.96 ± 0.02 eV, 368.21 ± 0.02 eV and 932.62 ± 0.02 eV. The Fermi-edge is calibrated with a polycrystalline Ni sample. The measurement resolution from this calibration is better than 0.2eV. The unfiltered He I (21.2 eV) photons are used for work function measurements under a bias of -5V.

Further Characterizations

Further characterizations of the samples are carried out using scanning electron microscope (SEM, JEOL JSM-6400F), Micro-Raman spectroscopy (Renishaw inVia 2000 with 532nm laser), atomic force microscope (Bruker Dimension FastScan) and a "Cascade Microtech" optical microscope.

Results and discussion

Formation and Raman Analysis of MoS_2 /CNTs Hybrid Material

To assemble few-layer n-type MoS_2 onto the supporting CNT scaffolds, the following steps as illustrated in **Figure 1(a)** are carried out. The size of all samples are approximately 2mm x 2mm while those used for UPS measurements are about 8mm x 8mm in size. First, using the method described in the Experimental Section, few-layer MoS_2 (with PMMA coating) is first floated in de-ionized (DI) water in a beaker. Subsequently, substrate that comprises aligned array of CNTs attached onto a holder is submerged into the beaker of water and then raised gently to scoop up the floating MoS_2 film. The CNTs sample that is dressed with the MoS_2 film is subsequently placed into

Nanoscale Accepted Manuscript

This journal is © The Royal Society of Chemistry 20xx

another beaker. To remove the PMMA coating on the MoS_2 film, acetone is added into the beaker. After 30 minutes, a syringe is used to extract the remaining acetone from the beaker and the MoS_2/CNTs sample is left to dry in ambient. The resultant clear film served as a proof for the complete removal of the PMMA coating.

Figure 1(b-c) shows top-view SEM images CNTs array taken (b) before and (c) after assembly of the MoS_2 film. After the assembly process, ripples and folds are observed on the MoS_2 film. In addition, it is notable that the few-layer MoS_2 film is thin enough such that the underlying CNT strands are still observable. A higher magnification SEM image as shown in Figure 1(d) clearly depicts the level of transparency of the MoS_2 film assembled on the CNTs array. Thickness of the MoS_2 film is determined from Atomic Force Microscopy (AFM) imaging of MoS_2 film that had been transferred onto Si substrate (Figure 1(f)). An average thickness of ~ 2.7 nm is obtained from the three regions indicated by the pink lines and blue crosses indicated in Figure 1(f). Given the reported thickness of single layer MoS_2 films as 6.5Å,[20] the film used in this experiment is estimated to be 4 layers thick.

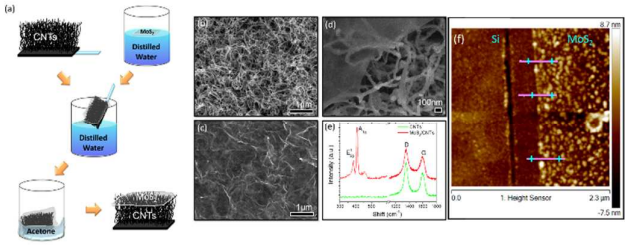

Figure 1. (a) Schematic of the assembly process to place few-layer MoS_2 over vertically aligned CNTs array. (b-e) Top-view SEM image of (b) as-grown CNTs, (c) few-layer MoS_2 covering the CNTs array and (d) edge of the MoS_2 film showing underlying CNTs array. (e) Raman spectra of CNTs and MoS_2/CNT hybrid. (f) AFM image of the MoS_2 film deposited on a silicon substrate. Pink lines and blue crosses indicate the regions from which average height of the film is obtained.

Being a non-destructive characterization tool, Raman spectroscopy is a key diagnostic tool for the characterization of graphene[21] and the investigation of strain effect on the G and 2D peaks.[22-25] Given the structural similarities between MoS_2 film and Graphene, it is thus a natural choice to use Raman spectroscopy for the characterization of the assembled MoS_2/CNTs hybrid material. Figure 1(e) shows the Raman spectra obtained for the assembled MoS_2/CNTs hybrid and CNTs respectively. Raman spectrum of CNTs exhibits the usual D band (~1351cm^{-1}) and G band (~1586cm^{-1}) at high wavenumber region[26]. The D band is attributed to the disordering in the graphitic layers or an amorphous carbon[27] while in-plane stretching, E_{2g} mode, contributed to the G band.

Raman spectrum of hybrid MoS_2/CNTs exhibits three additional bands at the low-wavenumber region in addition to the D and G bands. The three active bands at the lower wavenumber region of Raman spectrum for MoS_2/CNTs hybrid are associated to the E^1_{2g} mode (~384cm^{-1}),[28] the A_{1g} mode (~406cm^{-1})[28] and an asymmetric peak at ~451cm^{-1}.[29] The E^1_{2g} mode arises from in-layer displacements of the molybdenum sulfur atoms while the A_{1g} mode is linked to the out-of-layer symmetric displacements of sulfur atoms along the c-axis.[28] The sharpness of the E^1_{2g} Raman peak and the A_{1g} Raman peak is often used as an indicator of the high crystallinity of the MoS_2 film.[16] Presence of the asymmetric peak had been reported to be due to either the oxidation state of molybdenum or due to a superposition of the second-order process involving the longitudinal acoustic phonon scattering and Raman inactive A_{2u} mode, which can be activated by strong resonance effect.[29]

Similar to Raman spectrum for pure CNTs, the Raman spectrum for assembled MoS_2/CNTs hybrid also exhibits a D band and a G band. Ratio of the intensities of D and G bands (I_D/I_G) from the hybrid material is found to be ~1.12, while the I_D/I_G from pure CNT is ~1.31. Since the deposition of the MoS_2 film only occurs solely on the outer graphene layer of the MWNTs, no drastic changes to the carbon hybridization is expected. Thus the small decrement in the ratio of I_D/I_G for the hybrid material is within expectation and is in agreement with previous studies pertaining to covalently and non-covalently functionalized multi-walled CNTs.[30, 31]

Low Power Focused Laser Enabled Micro-crafting of MoS_2 on CNTs array

Following the successful dressing of the CNTs array with thin gauze of MoS_2, it would be desirable to be able to further pattern the thin gauze into a wide variety of micropatterns. Spatial arrangements and geometries of these micropatterns play an important role in the study of fundamental properties. In addition, the ability to create micro-dressing of the MoS_2 gauze on CNTs array can facilitate practical implementations of the hybrid material in electronic devices, it is thus essential to develop this patterning process. The challenge is to develop a technique that can exclusively modify or remove the MoS_2 gauze on the CNTs and yet leave the CNTs unscathed after the process.

To facilitate such a micro-crafting process, we make use of a facile focused laser pruning method. When the assembled MoS_2/CNTs hybrid sample is illuminated by a focused laser beam at low laser power, the MoS_2 film is found to disintegrate but the CNTs beneath it is totally unscathed. The focused laser beam is chosen on the basis that MoS_2 and CNTs react differently to laser beams of different wavelengths. MoS_2 is found to be more responsive to laser beam emitting light with a wavelength 532nm while CNTs are more affected by laser beam emitting light with a wavelength of 660nm. Thus a low power focused laser beam (with λ=532nm) is able to remove MoS_2 that is placed on top of CNTs array without affecting the CNTs underneath. On the other hand, we can use another focused laser beam (with λ = 660 nm) to create a wide

Nanoscale Accepted Manuscript

variety of CNTs patterned array before the assembly of the MoS_2 film. The flexibility to alter the wavelengths of the focused laser beam system renders it as an effective tool for selective removal of either the MoS_2 film or the underlying CNTs.

Figure 2(a) shows a schematic of the focused laser patterning setup used in this work. A 532nm or 660nm parallel laser beam is directed into an opening of a microscope using two mirrors. Reflecting off a beam splitter inside the microscope, part of the beam is sent through an objective lens and focused onto the sample. In this work, an objective lens with a magnification of 100x is used for the laser with λ = 532nm. On the other hand, an objective lens with a magnification of 50x is used for the laser with λ = 660nm. The sample is illuminated via an illumination light source (not shown in Figure 2) and part of the reflected light passes through the beam splitter and becomes collected by a CCD camera. Presence of the camera provided real-time imaging and monitoring of the patterning

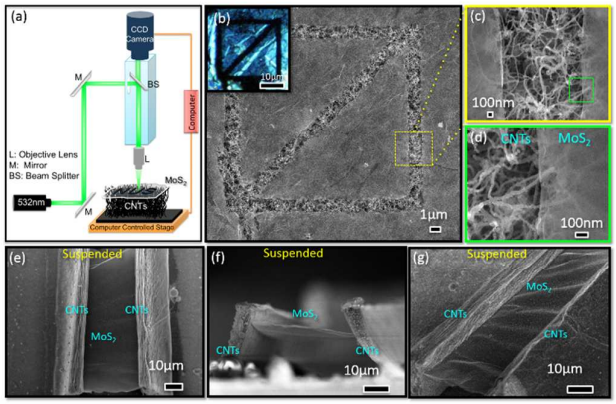

Figure 2. (a) Schematic (not to scale) of the focused laser patterning setup used in crafting the MoS_2 film. (b-d) Top-view SEM image of (b) patterned MoS_2 film on CNTs array (inset is the corresponding optical image); (c) higher magnification image of the region enclosed in the dotted yellow box in (b) and (d) junction between the cut MoS_2 film and underlying CNTs array. The image is obtained from the region enclosed in the green box shown in (c). (e-g) SEM images of MoS_2 film suspended across CNTs micro-platforms, taken at (e) top-view, (f) side-view and (g) 40° tilt.

Using the described technique (with 1.5mW of focused laser beam (λ = 532nm)) and setting the sample to move at 10μm/s, we use the focused laser beam to create a box by laser pruning and then prune a line from one corner to the other diagonal corner. This results into two right angled triangles as shown in Figure 2(b). Inset of Figure 2(b) shows corresponding optical image of the patterned MoS_2 film. High optical contrast between the underlying CNTs and the MoS_2 film provides a quick and efficient way of verifying any micro-pattern on the hybrid structure. Quality of the MoS_2 film after undergoing the patterning process is highlighted in Figure 2(c) and 2(d). Figure 2(c) reveals the supporting CNTs through a gap created on the MoS_2 film. Higher magnification image (Figure 2(d)) taken at the edge of the MoS_2 film (enclosed in the green box), shows a clean and clear cut portion of the MoS_2 film. Hence suggesting that this simple yet efficient patterning process is highly capable of producing good quality patterned MoS_2 gauze that rests on top of the CNTs array.

Given the selective responsiveness of the materials to different wavelengths, the patterning process is not limited to just the MoS_2 film. By changing the laser beam to 660nm with 60mW, pristine array of CNTs can be patterned into micro-platforms as supporting scaffold[12] before the assembly of the MoS_2 film. Using the same assembly method described in Figure 1(a), the MoS_2 film is assembled across the CNTs micro-platforms and SEM image of the assembled structure is shown in Figure 2(e). The MoS_2 film is suspended across flexible CNT scaffolds (Figure 2(f)). In this way, substrate induced influence on various properties (such as electronic properties) of the MoS_2 film is eliminated. Furthermore, ripples induced on the MoS_2 film (Figure 2(g)) provide an avenue for bandgap engineering processes[32] to be further investigated. With the patterning tool developed, 3D supporting CNT architectures can be varied and hence offers an opportunity to conduct detailed studies on the stress and strain relationship between the supporting structures and the MoS_2 film. Investigation into this relationship is currently ongoing and details will be provided in a separate report.

Raman Analyses of Micro-crafted of MoS_2 on CNTs array

With the MoS_2 film and CNTs in close proximity, it is important to have a fundamental understanding of the interaction between the MoS_2 film and the CNTs strands before the full potential of this hybrid material can be realized. Non-destructive Raman spectroscopy is utilized as a probe to undertake this study. Out of the three active bands of the MoS_2/CNTs Raman spectrum (Figure 1(e)), we focus our attention on the E^1_{2g} mode (~384cm^{-1})[28] and the A_{1g} mode (~406cm^{-1})[28]. The E^1_{2g} mode is highly sensitive to long-range interlayer Coulombic interaction between the molybdenum atoms from different layers of MoS_2 film.[7] As a result, a few factors have been reported to account for the shift towards lower frequency that has been observed in this mode. Namely, (1) increase in dielectric tensor arising from increase of film thickness,[33] (2) application of external strain[34] and (3) increase in film temperature.[35, 36] The A_{1g} mode is determined to be highly responsive to adsorbates on the MoS_2 surface[37] and electron doping.[38] With this responsiveness arising from strong electron-phonon coupling, increase in doping level and rise of film temperature can cause the A_{1g} mode to undergo a shift towards lower frequency. At the same time, this shift is accompanied by an increase in the peak width.

For the Raman studies, first we fabricate a sample comprising of few-layer MoS_2 film on a flat substrate made of SiO_2 on Si. This sample serves as a reference sample and Raman spectrum of the MoS_2 film is captured from this reference sample. **Figure 3(a)** shows the two Raman spectra obtained from MoS_2 on CNTs and MoS_2 on SiO_2/Si respectively. Compared to the MoS_2

Nanoscale Accepted Manuscript

This journal is © The Royal Society of Chemistry 20xx

film that is assembled on SiO_2 substrate, placing the film over CNTs causes a pronounced shift towards lower frequency in the E^1_{2g} mode by ~ 4cm^{-1}. From the same sample, similar shift towards lower frequency in the A_{1g} mode (~ 3cm^{-1}) is also observed. Not only is there observable shift in the mode, an increase in the full width half maximum (FWHM) (~ 4cm^{-1}) of the mode is also detected. With temperature being maintained at a constant level throughout the detection process, we can narrow down the cause to changes in the electron doping level of the MoS_2 film upon interacting with the underlying CNTs support. For this claim to hold true, we should be able to detect changes to the electronic structure of the CNTs. This change is supported by a shift towards lower frequency in the G band of the CNTs as shown in Figure 3(b). From Figure 3(b), only CNTs that are in contact with the MoS_2 film experienced a shift towards lower frequency by ~ 8cm^{-1} in the G band.

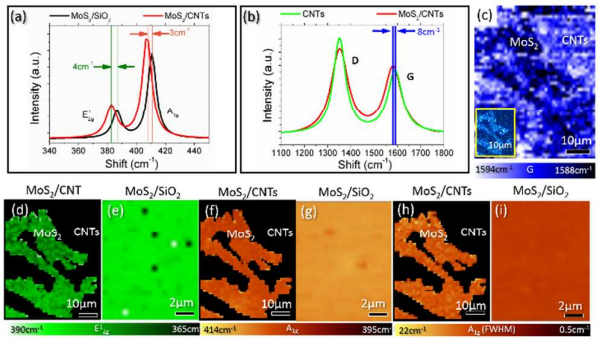

Figure 3. (a) Raman spectra of E^1_{2g} and A_{1g} mode of MoS_2/CNTs film and the MoS_2 film on SiO_2 substrate. (b) Raman spectra of D and G mode of MoS_2/CNTs film and the underlying CNTs. (c-i) Raman map of (c) G mode, (d-e) E^1_{2g} mode, (f-g) A_{1g} mode and (h-i) FWHM of the A_{1g} mode of laser patterned, "dragon", MoS_2/CNTs film and the MoS_2 film on SiO_2 substrate. Inset of (c) shows the corresponding optical image of the "dragon" pattern used for the Raman map.

Combining the attribute of the Raman shift and the ability to create micro-pattern via laser pruning, we can create laser pruned micro-pattern of MoS_2 on CNTs and then capture Raman map of these micropatterns. As an example, we make use of laser pruning to create a "dragon" pattern on MoS_2 on CNTs and then study the corresponding Raman map. Figure 3(c) shows Raman map of the micropattern with the window centered at the G band of CNTs. The inset found at the lower left corner of Figure 3(c) shows an optical image of the patterned MoS_2 film used for analysis. Figures 3(d-i) show Raman maps of both the "dragon" patterned MoS_2/CNTs and MoS_2/SiO_2 samples. Compared to the MoS_2 film that is assembled on SiO_2 substrate, placing the film over CNTs causes a pronounced shift towards lower frequency in the E^1_{2g} mode by ~ 4cm^{-1}. In Figure 3(d-e), the Raman maps are obtained with the window centered at around the E^1_{2g} mode of MoS_2. In Figure 3(f-g), the Raman maps are obtained with the window centered at around the A_{1g} mode of MoS_2. In Figure 3(h-i), the Raman maps are obtained with the window centered on the FWHM of the Raman peak for A_{1g} mode of MoS_2. Given the uniformity of the film and that no additional heating is introduced on the sample (laser power of the Raman system is maintained at 340μW throughout the measurement process), the shift towards lower frequency is attributed to the application of strain on the MoS_2 film. Presence of external strain can be induced by entanglement of the CNTs at the surface of the array (Figure 1(b)). Given the flexibility of MoS_2 film, it can easily mold itself to the features present on the surface of the array. This in turn results in the formation of ripples on the film (Figure 1(c)), which can play a significant role in shifting the frequency of the E^1_{2g} mode.

Further investigations into how CNTs can affect the degree of electron doping, as well as straining on the MoS_2 film, are carried out using CNTs of different densities. CNTs array with higher density provides more contact points between the CNTs and the MoS_2 film. These contact points could increase the amount of electron doping and also induce more strain on the MoS_2 film. This in turn can lead to a higher degree of shift towards lower frequency in the E^1_{2g}, A_{1g} and G peaks detected. **Figure 4(a-b)** shows side view SEM images of high density (CNTs/HD) and low density (CNTs/LD) CNTs. The number density of CNTs/HD was 1.94x10^{13} m^{-2} while that of CNTs/LD was 1.18x10^{13} m^{-2}.

For fair comparison, MoS_2 film obtained from the same piece of sample is placed onto CNT arrays of different densities. As a

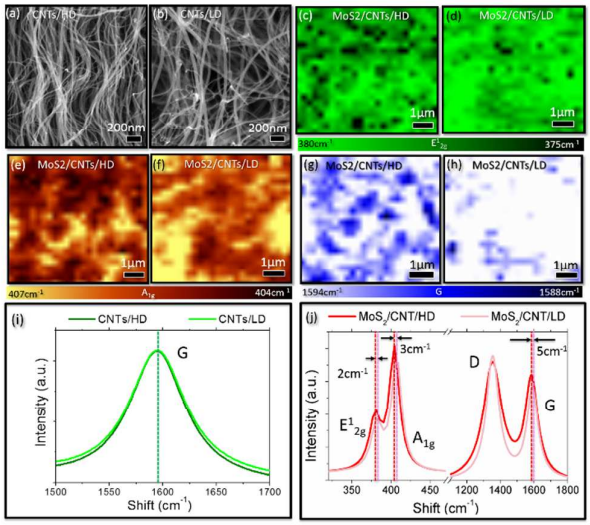

Figure 4. Side view SEM images of (a) high and (b) low density CNTs. (c-h) Raman maps of MoS_2 film on high and low density CNTs with mapping window at (c-d) E^1_{2g}, (e-f) A_{1g} and (g-h) G mode respectively. (i) Raman spectra showing G mode of the CNTs samples before the transfer of MoS_2 film. (j) Raman spectra showing E^1_{2g}, A_{1g}, peaks of the MoS_2 film and D, G mode of the CNTs samples after the assembly of MoS_2 film.

Nanoscale Accepted Manuscript

Raman spectra obtained from both samples, before the assembly of MoS_2 film, shows no significant shift in the G mode (Figure 4(i)). In comparison, Raman spectra showed significant shift towards lower frequency (~5cm^{-1}) in the G mode from MoS_2 film placed onto high density CNTs (MoS_2/CNT/HD). This is in comparison to that placed onto lower density of CNTs array (MoS_2/CNT/LD). Similarly, shift of 2cm^{-1} in the E^1_{2g} peak and 3cm^{-1} in the A_{1g} peak towards the lower frequency range could be detected from the MoS_2/CNT/HD. This is in comparison to the MoS_2/CNT/LD sample. The results from the Raman analyses thus supported the above suggestions that the presence of more contact points between the MoS_2 film and the supporting CNTs could induced more strain, as well as electron doping.

CNTs array provides a large number of contact points between the CNTs and the MoS_2 film. As shown in the SEM image in Figure 5(a), the MoS_2 film is in very good contact with the CNT strands. These contact points represent regions with interfaces whereby the energy levels of the composite materials become modified. To provide further insight into the modification of the energy diagram after the assembly of the hybrid materials, UPS measurements are conducted on the hybrid material (Figure 5(b)). By extrapolating the cutoff point to the horizontal axis (inset), work functions of Si, MoS_2/Si, MoS_2/CNTs, and CNTs are determined to be 3.49eV, 3.83eV,

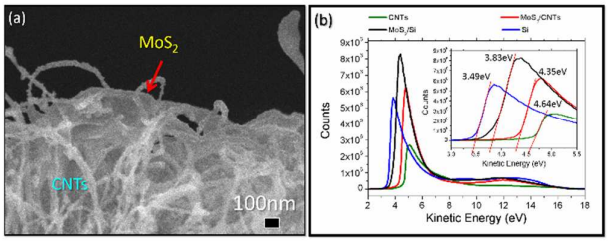

Figure 5. (a) SEM image showing multiple contact points between the MoS_2 film and the supporting CNT strands. (b) UPS data showing the respective work function of Si, MoS_2/Si, MoS_2/CNTs, and CNTs at 3.49eV, 3.83eV, 4.35eV and 4.64eV. The work functions are obtained by extrapolating the cutoff point to the horizontal axis (inset).

Current-Voltage Measurements and Optoelectric Effect of MoS_2 /CNTs Hybrid Material

The capability of the hybrid material to engage in opto-electric conversion is tested using top-down, two probes technique. A schematic of this measurement process is illustrated in Figure 6(a). Tungsten probes from a probe-station were utilized to achieve contact with the assembled sample. The negative terminal was located at the MoS_2 film while the positive terminal was connected to the Silicon (Si) substrate. From a work published by Gourmelon *et al.*, an ohmic contact was obtained from a tungsten (W) -MoS_2-tungsten sample. The contact resistance was found to be smaller than the resistance of the MoS_2 film.[39] With the Si substrate being negatively

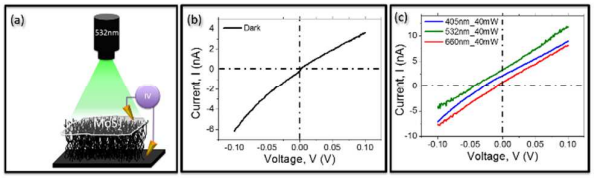

of the tested area was measured using image analysis software. All I-V data presented is an average obtained from 3 different readings and taken in ambient condition.

Figure 6. (a) Schematic of the setup used for optoelectric measurements. (b-c) Top-down, two probe I-V measurements of the MoS_2/CNTs hybrid material (b) without and (c) with external illumination.

Figure 6(b) shows I-V characteristic of the MoS_2/CNTs hybrid measured without illumination. At 0V, no current is detected from the sample. Illuminating the sample with broad beam lasers of different wavelengths (405nm, 532nm and 660nm) resulted in upward shifts of the I-V graphs obtained (Figure 6(c)). Power of all lasers is kept at 40mW. Note that with a broad laser beam (diameter ~ 2-3mm), the laser intensity is insufficient to cause any damage to the sample. The most significant shift in the I-V graph is observed when the 532nm laser is introduced onto the sample. This gives rise to a photocurrent of 3.49nA at 0V. Given that both W-MoS_2 and W-Si contacts show ohmic behavior, it is thus possible for us to identify the MoS_2/CNTs hybrid material as the source of the photocurrent detected.

To demonstrate the material's capability to engage in photo-electric conversion, we conducted current-time (I-t) measurements on the sample. Using similar experimental setup as that mentioned above, current measurements are carried out while exciting the sample at 10s intervals with lasers of different wavelengths. Throughout the measurement process, a 0.1V bias is applied onto the sample. The photo-response curves presented in **Figure 7(a)** shows three separate photo-response processes. The responses are associated to excitation from laser sources emitting laser light with a wavelength of 405nm, 532nm and 660nm respectively. Once illuminated with the excitation source, a rapid rise in the current is detected. Under 660nm excitation, maximum current is achieved in 0.1s, whereas 0.2s is required when the excitation source is changed to 405nm and 532nm. We believe that the measured response time is limited by the

Nanoscale Accepted Manuscript

This journal is © The Royal Society of Chemistry 20xx

measurement unit used. The rapid responses observed upon introduction of external excitation is more skewed towards photovoltaic effect in comparison to the thermal and optically induced photocurrent reported by Perea-López *et al*.[40] Excitation with laser light with a wavelength of 532nm results in a change in current (δI) of ~7nA. This is followed by a change in current of ~5nA and ~3nA upon excitation with laser light with wavelengths of 405nm and 660nm.

Photo-responsiveness of the MoS_2/CNTs hybrid materials is further emphasized in the power dependent photo-response curves as illustrated in Figure 7(b-d). Power of each excitation laser is varied from 60mW, 40mW and 20mW. In general, increasing the power of the excitation source will result in an

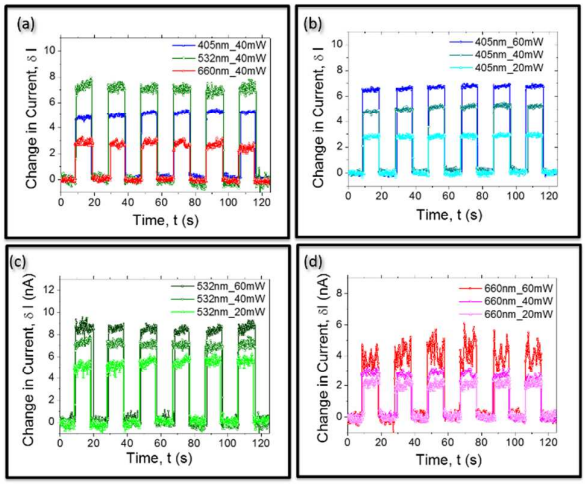

Figure 7. (a) Photo-response, I-t graphs obtained from MoS_2/CNTs hybrid material under illumination from 405nm, 532nm and 660nm, with a fixed laser power of 40mW. (b-d) Photo-response, I-t graphs obtained from (b) 405nm, (c) 532nm and (d) 660nm with varying excitation powers of 60mW, 40mW and 20mW.

From the above results presented, we believe that the observed photocurrent could be a result of both photothermoelectric (PTE) and photovoltaic (PVE) effects from the hybrid material. In general, we believe that charge carriers will be generated from the MoS_2 film and at the interfaces between the film and the supporting CNT strands. Subsequently, these charge carriers will be transported to the Si substrate by the metallic CNTs array.

Consider MoS_2 as the material, first principle theoretical study[41] on the thermoelectric effect of few-layer n-type MoS_2 suggested decreasing thermoelectric efficiency in the MoS_2 as the thickness increases. Since the MoS_2 film used in our study comprised of 4-layer n-type MoS_2 film, it is reasonable to believe that PTE is not as significant as PVE from the MoS_2 film alone in our hybrid material. Apart from having charge carriers generated from the MoS_2 film, these charge carriers can also be generated at the interfaces between the film and the supporting CNTs.

In a recent work by Zhang *et al*, [8] they identified that at the MoS_2-metal interface, photocurrent was determined to originate from PVE while hot-carrier assisted PTE was more dominant in the depletion regime. With multiple contact points being established between the MoS_2 film gauzing over the MWNT supporting strands (Figure 5(a)), PVE is expected to be a significant contributing factor to the observed photocurrent detected. This deduction is consistent with the rapid response detected in the I-t graphs presented in Figure 7. However we cannot rule out the contributions of PTE at the interface as emphasized by Zhang *et al*.

The charge carriers generated in the film and at the interfaces will then be transported to the Si substrate *via* the supporting metallic multi-walled CNTs. In this study, only metallic multi-walled CNTs (MWNTs) grown on n-type Si substrate are used as the supporting structure for the MoS_2 film. Interestingly, photocurrent has been reported to be detected from suspended metallic CNTs. Source of the photocurrent was determined to arise from photo-excited hot carriers in the material.[42] In our case, we believe that this effect in the metallic CNTs will have minimal contribution to the overall photoelectric effect. This is because, the as-grown MWNTs were attached to the n-type Si substrates, which they were synthesized on. This substrate will serve as a heat sink which could suppress the PTE arising from the supporting MWNTs.

While both the MoS_2 film and the supporting Si substrate are both semi-conductors, the densely packed CNTs array could have shielded the substrate from the excitation source. Hence minimising any photoelectric effect arising from the supporting substrate.

Conclusion

In summary, unique 3D hybrid material comprising of few-layer MoS_2 gauze assembled onto vertically aligned CNTs array has been created. Using a focused laser beam with different wavelengths, site selective patterning of either the MoS_2 film or the supporting CNTs array is achieved. This paves the way for applications and investigations into the fundamental properties of the hybrid MoS_2/CNTs material. Through Raman mapping, straining and electron doping of MoS_2 film as a result of interaction with the supporting CNTs array are detected. Role of the CNTs is further emphasized, with higher density CNTs (hence providing more electrical contact points with the MoS_2 film) resulting in a more significant shift in the G peak of the Raman spectrum. Photo-response measurements are successful in detecting optoelectronic behavior of the hybrid

Nanoscale Accepted Manuscript

material. At 0V, 3.49nA of current is measured upon illuminating the sample with a broad beam 532nm laser. With its swift response to external irradiation of different wavelength and different excitation powers, the hybrid material has shown potential for applications in light harnessing devices.

Acknowledgements

The authors would like to acknowledge the support of the MOE ARC Tier 2 grant (WBS: R-144-000-338-112).

References

1. J. Yang, J. Y. Lee and H. P. Too, *Analytica Chimica Acta*, 2005, **546**, 133-138.
2. Y. Ma, M. G. Zhao, B. Cai, W. Wang, Z. Z. Ye and J. Y. Huang, *Biosensors & Bioelectronics*, 2014, **59**, 384-388.
3. R. L. Vander Wal and L. J. Hall, *Carbon*, 2003, **41**, 659-672.
4. P. C. Ma, B. Z. Tang and J. K. Kim, *Carbon*, 2008, **46**, 1497-1505.
5. K. F. Mak, C. Lee, J. Hone, J. Shan and T. F. Heinz, *Physical Review Letters*, 2010, **105**, 4.
6. A. Splendiani, L. Sun, Y. B. Zhang, T. S. Li, J. Kim, C. Y. Chim, G. Galli and F. Wang, *Nano Letters*, 2010, **10**, 1271-1275.
7. R. Ganatra and Q. Zhang, *Acs Nano*, 2014, **8**, 4074-4099.
8. Y. W. Zhang, H. Li, L. Wang, H. M. Wang, X. M. Xie, S. L. Zhang, R. Liu and Z. J. Qiu, *Scientific Reports*, 2015, **5**.
9. P. Avouris, T. Hertel, R. Martel, T. Schmidt, H. R. Shea and R. E. Walkup, *Applied Surface Science*, 1999, **141**, 201-209.
10. S. Frank, P. Poncharal, Z. L. Wang and W. A. de Heer, *Science*, 1998, **280**, 1744-1746.
11. Y. Yu, C. H. Jin, R. H. Wang, Q. Chen and L. M. Peng, *Journal of Physical Chemistry B*, 2005, **109**, 18772-18776.
12. K. Y. Lim, C. H. Sow, J. Y. Lin, F. C. Cheong, Z. X. Shen, J. T. L. Thong, K. C. Chin and A. T. S. Wee, *Advanced Materials*, 2003, **15**, 300-303.
13. A. Taube, J. Judek, C. Jastrzebski, A. Duzynska, K. Switkowski and M. Zdrojek, *Acs Applied Materials & Interfaces*, 2014, **6**, 8959-8963.
14. X. D. Lim, H. W. G. Foo, G. H. Chia and C. H. Sow, *Acs Nano*, 2010, **4**, 1067-1075.
15. N. Chakrapani, B. Q. Wei, A. Carrillo, P. M. Ajayan and R. S. Kane, *Proceedings of the National Academy of Sciences of the United States of America*, 2004, **101**, 4009-4012.
16. V. O. Koroteev, L. G. Bulusheva, I. P. Asanov, E. V. Shlyakhova, D. V. Vyalikh and A. V. Okotrub, *Journal of Physical Chemistry C*, 2011, **115**, 21199-21204.
17. Y. M. Shi, Y. Wang, J. I. Wong, A. Y. S. Tan, C. L. Hsu, L. J. Li, Y. C. Lu and H. Y. Yang, *Scientific Reports*, 2013, **3**, 8.
18. A. Rizzo, R. Rossi, M. A. Signore, E. Piscopiello, L. Capodieci, R. Pentassuglia, T. Dikonimos and R. Giorgi, Berlin, GERMANY, 2007.
19. K. K. Liu, W. J. Zhang, Y. H. Lee, Y. C. Lin, M. T. Chang, C. Su, C. S. Chang, H. Li, Y. M. Shi, H. Zhang, C. S. Lai and L. J. Li, *Nano Letters*, 2012, **12**, 1538-1544.
20. B. Radisavljevic, A. Radenovic, J. Brivio, V. Giacometti and A. Kis, *Nature Nanotechnology*, 2011, **6**, 147-150.
21. A. C. Ferrari, *Solid State Communications*, 2007, **143**, 47-57.
22. O. Frank, M. Mohr, J. Maultzsch, C. Thomsen, I. Riaz, R. Jalil, K. S. Novoselov, G. Tsoukleri, J. Parthenios, K. Papagelis, L. Kavan and C. Galiotis, *Acs Nano*, 2011, **5**, 2231-2239.
23. O. Frank, G. Tsoukleri, J. Parthenios, K. Papagelis, I. Riaz, R. Jalil, K. S. Novoselov and C. Galiotis, *Acs Nano*, 2010, **4**, 3131-3138.
24. G. Tsoukleri, J. Parthenios, K. Papagelis, R. Jalil, A. C. Ferrari, A. K. Geim, K. S. Novoselov and C. Galiotis, *Small*, 2009, **5**, 2397-2402.
25. C. C. Chen, W. Z. Bao, J. Theiss, C. Dames, C. N. Lau and S. B. Cronin, *Nano Letters*, 2009, **9**, 4172-4176.
26. T. Belin and F. Epron, *Materials Science and Engineering B-Solid State Materials for Advanced Technology*, 2005, **119**, 105-118.
27. M. S. Dresselhaus, A. Jorio, A. G. Souza and R. Saito, *Philosophical Transactions of the Royal Society a-Mathematical Physical and Engineering Sciences*, 2010, **368**, 5355-5377.
28. Q. Li, E. C. Walter, W. E. van der Veer, B. J. Murray, J. T. Newberg, E. W. Bohannan, J. A. Switzer, J. C. Hemminger and R. M. Penner, *Journal of Physical Chemistry B*, 2005, **109**, 3169-3182.
29. G. L. Frey, R. Tenne, M. J. Matthews, M. S. Dresselhaus and G. Dresselhaus, *Physical Review B*, 1999, **60**, 2883-2892.
30. V. Georgakilas, A. Bourlinos, D. Gournis, T. Tsoufis, C. Trapalis, A. Mateo-Alonso and M. Prato, *Journal of the American Chemical Society*, 2008, **130**, 8733-8740.
31. K. Kardimi, T. Tsoufis, A. Tomou, B. J. Kooi, M. I. Prodromidis and D. Gournis, *International Journal of Hydrogen Energy*, 2012, **37**, 1243-1253.
32. J. Qi, X. Li, X. Qian and J. Feng, *Applied Physics Letters*, 2013, **102**.
33. A. Molina-Sanchez and L. Wirtz, *Physical Review B*, 2011, **84**, 8.
34. Y. L. Wang, C. X. Cong, C. Y. Qiu and T. Yu, *Small*, 2013, **9**, 2857-2861.
35. N. A. Lanzillo, A. G. Birdwell, M. Amani, F. J. Crowne, P. B. Shah, S. Najmaei, Z. Liu, P. M. Ajayan, J. Lou, M. Dubey, S. K. Nayak and T. P. O'Regan, *Applied Physics Letters*, 2013, **103**, 4.
36. S. Najmaei, Z. Liu, P. M. Ajayan and J. Lou, *Applied Physics Letters*, 2012, **100**, 4.
37. W. J. Zhang, J. K. Huang, C. H. Chen, Y. H. Chang, Y. J. Cheng and L. J. Li, *Advanced Materials*, 2013, **25**, 3456-3461.
38. B. Chakraborty, A. Bera, D. V. S. Muthu, S. Bhowmick, U. V. Waghmare and A. K. Sood, *Physical Review B*, 2012, **85**, 4.
39. E. Gourmelon, J. C. Bernede, J. Pouzet and S. Marsillac, *Journal of Applied Physics*, 2000, **87**, 1182-1186.
40. N. Perea-López, Z. Lin, N. R. Pradhan, A. Iñiguez-Rábago, A. L. Elías, A. McCreary, J. Lou, P. M. Ajayan, H. Terrones and L. Balicas, *2D Materials*, 2014, **1**.
41. W. Huang, X. Luo, C. K. Gan, S. Y. Quek and G. C. Liang, *Physical Chemistry Chemical Physics*, 2014, **16**, 10866-10874.
42. M. Barkelid and V. Zwiller, *Nature Photonics*, 2014, **8**, 48-52.

Nanoscale Accepted Manuscript

This journal is © The Royal Society of Chemistry 20xx

Please do not adjust margins

Nanoscale Accepted Manuscript

This journal is © The Royal Society of Chemistry 20xx

Please do not adjust margins